Journal of Solid State Chemistry 183 (2010) 2910–2916

Contents lists available at ScienceDirect

Journal of Solid State Chemistry

journal homepage: www.elsevier.com/locate/jssc

Synthesis, crystal structure, spectrum properties, and electronic structure of a novel non-centrosymmetric borate, $BiCd_3(AlO)_3(BO_3)_4$

Xuean Chen [a,*], Hui Yin [a], Xinan Chang [a], Hegui Zang [a], Weiqiang Xiao [b]

[a] College of Materials Science and Engineering, Beijing University of Technology, Ping Le Yuan 100, Beijing 100124, PR China
[b] Institute of Microstructure and Property of Advanced Materials, Beijing University of Technology, Beijing 100124, PR China

ARTICLE INFO

Article history:
Received 7 July 2010
Received in revised form
2 September 2010
Accepted 22 September 2010
Available online 29 September 2010

Keywords:
$BiCd_3(AlO)_3(BO_3)_4$
Borate
Crystal structure
Band structure

ABSTRACT

A novel non-centrosymmetric borate, $BiCd_3(AlO)_3(BO_3)_4$, has been prepared by solid state reaction methods below 750 °C. Single-crystal XRD analysis showed that it crystallizes in the hexagonal group $P6_3$ with $a=10.3919(15)$ Å, $c=5.7215(11)$ Å, $Z=2$. In its structure, AlO_6 octahedra share edges to form 1D $^1_\infty[AlO_4]^{5-}$ chains that are bridged by BO_3 groups through sharing O atoms to form the 3D $^3_\infty[AlBO_4]^{2-}$ framework. The 3D framework affords two kinds of channels that are occupied by Bi^{3+}/Cd^{2+} atoms only or by Bi^{3+}/Cd^{2+} atoms together with BO_3 groups. The IR spectrum further confirmed the presence of BO_3 groups. Second-harmonic-generation measurements displayed a response of about $0.5\times$ KDP (KH_2PO_4). UV–vis diffuse reflectance spectrum showed a band gap of about 3.19 eV. Solid-state fluorescence spectrum exhibited the maximum emission peak at around 390.6 nm. Band structure calculations indicated that it is an indirect semiconductor.

1. Introduction

In the past decades, borate materials have been widely investigated because they have important practical applications in second harmonic generation (SHG). For example, β-BaB_2O_4, LiB_3O_5, CsB_3O_5, and $YCa_4(BO_3)_3O$ are all well-known nonlinear optical (NLO) crystals [1]. Bismuth-containing borates are of considerable interest because of the presence of Bi^{3+} $6s^2$ electron lone pairs is favorable for the formation of noncentrosymmetrical crystalline phases, which is pre-requisite for a variety of technologically important properties including ferroelectricity, piezoelectricity, pyroelectricity, and second-order nonlinear optical behavior.

The binary Bi_2O_3–B_2O_3 phase diagram has been examined by Levin and McDaniel [2], and at least six thermodynamically stable phases have been proposed including $Bi_{24}B_2O_{39}$ [3], $Bi_4B_2O_9$ [4], $Bi_3B_5O_{12}$ [5], BiB_3O_6 [6], α- and β-$Bi_2B_8O_{15}$ [7,8]. Among them, $Bi_4B_2O_9$ was reported to have high double-refraction [9], $Bi_3B_5O_{12}$ displays stimulated Raman scattering and luminescence properties [10,11], and BiB_3O_6 is the most extensively studied because it has been established as a NLO material with promising physical properties [12]. Theoretical studies have shown that the presence of irregular Bi–O coordination polyhedra and their favorable structural arrangement lead to the extraordinarily large optical SHG effect in BiB_3O_6 [13]. It is reasonable to emphasize that other interesting materials may also be found in more complex borates incorporating bismuth together with other cationic elements. Based on this idea, several ternary bismuth-containing borates that crystallize in the non-centrosymmetric space groups have been recently synthesized, including $BaBiBO_4$, $Bi_2ZnB_2O_7$, $Bi_2CaB_2O_7$, and $Bi_2SrB_2O_7$ [14–16]. In contrast to many investigations that have been done on the binary or ternary bismuth-containing borates mentioned above, the quaternary borates incorporating bismuth together with two kinds of other cationic elements are less explored. In the literature, only one quaternary bismuth-containing borate, $CaBiGaB_2O_7$, has been structurally characterized [15].

In the course of our investigation of novel borate NLO materials, we have obtained a new quaternary bismuth-containing borate, $BiCd_3(AlO)_3(BO_3)_4$, which is the first quaternary borate to be discovered in the Bi_2O_3–CdO–Al_2O_3–B_2O_3 system and crystallizes in a non-centrosymmetric, chiral space group $P6_3$. To the best of our knowledge, there are no experimental measurements of XRD, IR, UV–vis diffuse reflectance, and fluorescence spectra and also no first principle calculations on the electronic and optical properties of $BiCd_3(AlO)_3(BO_3)_4$ available in the literature. Therefore a combined experimental and theoretical study of $BiCd_3(AlO)_3(BO_3)_4$ is timely and would help in understanding the origin of the electronic properties. In this work we will present synthesis and characterization of this compound for the first time.

2. Experimental

2.1. Syntheses

The title compound was synthesized by employing high-temperature solid state reaction methods. All reagents were of

* Corresponding author.
E-mail addresses: xueanchen@bjut.edu.cn, xu_jiang_2002@yahoo.com (X. Chen).

0022-4596/$ - see front matter © 2010 Elsevier Inc. All rights reserved.
doi:10.1016/j.jssc.2010.09.030

analytical grade. For the preparation of $BiCd_3(AlO)_3(BO_3)_4$ crystals, a powder mixture of 0.9667 g Bi_2O_3, 0.5328 g CdO, 0.3237 g $Al(OH)_3$, and 0.2889 g B_2O_3 (Bi_2O_3/CdO/$Al(OH)_3$/B_2O_3 molar ratio=1:2:2:2) was transferred to a 10 mL Au crucible. The sample was gradually heated to 750 °C, where it was kept for 4 weeks, then cooled down to 700 °C at a rate of 0.5 °C/h, followed by cooling to room temperature at a rate of 20 °C/h. The colorless, prismatic crystals of $BiCd_3(AlO)_3(BO_3)_4$ were observed on the surface regions of the sample contacting the wall of the Au crucible. Several small crystals were recovered and mechanically separated from the reaction product. Energy-dispersive X-ray analyses in a scanning electron microscope confirmed the presence of heavy elements of bismuth, cadmium, and aluminum with an approximate atomic ratio of 1:3:3 in the crystals. Subsequently, direct reaction of a stoichiometric mixture of Bi_2O_3, CdO, $Al(OH)_3$, and H_3BO_3 at 600 °C for 4 weeks with several intermediate grindings yielded a single-phase polycrystalline sample as identified by powder XRD analyses, which further confirms the existence of this phase. This compound is relatively stable in air and water, but soluble in hot diluted HNO_3 solution.

2.2. Structure determination

Single-crystal X-ray intensity data were collected at room temperature (290 K) on an automated Rigaku AFC7R four-circle diffractometer using monochromatized Mo$K\alpha$ radiation (λ= 0.71073 Å). The data were corrected for Lorentz and polarization effects, and for absorption by empirical method based on ψ-scan data. The crystal structure was solved by direct methods and refined in SHELX-97 system [17] by full-matrix least-squares methods on F_o^2. After introduction of anisotropic displacement parameters for heavy atoms (Bi, Cd, and Al) and isotropic displacement parameters for light atoms (B and O), the refinement of 50 parameters with 935 observed reflections [$I \geq 2\sigma(I)$] resulted in the residuals of R_1/wR_2=0.0260/0.0640. The final difference electron density map was featureless, with the highest electron density less than 1.224 e Å^{-3}. Details of crystal parameters, data collection and structure refinements are given in Table 1 and the atomic coordinates and the equivalent isotropic displacement parameters are summarized in Table 2.

During the structural refinements of $BiCd_3(AlO)_3(BO_3)_4$, Al, B, and O atoms are well resolved, while Bi and Cd atoms were found to occupy two remaining atomic sites. Refinements of atomic occupancy parameters for these two positions gave the compositions $Bi_{0.2105(6)}Cd_{0.7895(6)}$ and $Bi_{0.3685(18)}Cd_{0.6315(18)}$, respectively, which leads to the final formula $BiCd_3Al_3B_4O_{15}$. The Bi^{3+}/Cd^{2+} disorder is not surprising because both Bi and Cd atoms have similar coordination geometries and Bi–O and Cd–O bond lengths are also very similar. The fact that Bi and Cd atoms occupy the same atomic sites has also been previously observed in many compounds such as $Bi_2Cd_4O_7$ [18], $Bi_{0.78}Cd_{0.22}VO_{3.72}$ [19], $Bi_{12.162}Cd_{1.838}V_4O_{30}$ [20], $Bi_{19.427}Cd_{3.573}V_4O_{42}$ [21], and $Bi_{3.785}Cd_{3.3}Cu_{1.775}(PO_4)_{3.5}O_{5.5}$ [22]. All of our attempts to refine this structure in lower-symmetry space groups with an ordered distribution of Bi and Cd atoms have been unsuccessful. An examination of the $BiCd_3(AlO)_3(BO_3)_4$ crystal with a slower scan rate and lower intensity limitation on a Rigaku AFC7R four-circle diffractometer did not indicate symmetry lower than hexagonal or a larger unit cell that would allow Bi/Cd ordering, therefore, the Bi^{3+}/Cd^{2+} disorder model was finally assumed.

Table 1
Crystallographic data for $BiCd_3(AlO)_3(BO_3)_4$.

Formula	$BiCd_3(AlO)_3(BO_3)_4$
Formula weight	910.36
Crystal size (mm^3)	0.15 × 0.05 × 0.05
Space group	$P6_3$ (No. 173)
a (Å)	10.3919(15)
c (Å)	5.7215(11)
V (Å^3), Z	535.09(15), 2
d_{calc} (g/cm^3)	5.650
μ (mm^{-1})	22.628
$2\theta_{max}$ (deg)	59.98
Unique reflection	1047
Observed [$I \geq 2\sigma(I)$]	935
No. of variables	50
GOF on F_o^2	1.063
R_1/wR_2 [$I \geq 2\sigma(I)$]	0.0260/0.0640
R_1/wR_2 (all data)	0.0319/0.0667

Table 2
Atomic coordinates and equivalent isotropic displacement parameters (Å^2) for $BiCd_3(AlO)_3(BO_3)_4$.

Atoms	*X*	*Y*	*Z*	U_{eq}
*M*1	0.14419(4)	0.29576(4)	0.7061(3)	0.01064(13)
*M*2	1/3	2/3	0.7040(4)	0.00852(15)
Al1	0.4967(9)	0.4989(13)	0.4470(12)	0.0026(4)
B1	0.4484(7)	0.2289(7)	0.696(4)	0.0034(13)
B2	0	0	0.901(2)	0.0070(13)
O1	0.4302(4)	0.0861(4)	0.699(3)	0.0048(8)
O2	0.4699(11)	0.3027(11)	0.9132(18)	0.007(2)
O3	0.4524(11)	0.2970(11)	0.4972(18)	0.008(2)
O4	0.3828(4)	0.4783(4)	0.711(3)	0.0047(8)
O5	0.1505(7)	0.0967(7)	0.8842(9)	0.009(2)

Note: *M*1 and *M*2 have the compositions $Bi_{0.2105(6)}Cd_{0.7895(6)}$ and $Bi_{0.3685(18)}Cd_{0.6315(18)}$, respectively. U_{eq} is defined as one-third of the trace of the orthogonalized U tensor.

As mentioned above, the crystals have been checked by energy-dispersive X-ray analyses (EDX) in a scanning electron microscope, which showed the presence of heavy elements of bismuth, cadmium, and aluminum. Moreover, a powder mixture of Bi_2O_3, CdO, $Al(OH)_3$, and H_3BO_3 [calculated from the composition $BiCd_3(AlO)_3(BO_3)_4$] was heated at 600 °C for 4 weeks with several intermediate grindings. The powder XRD pattern of the as-prepared sample is in agreement with that simulated from single-crystal data, confirming the existence of $BiCd_3(AlO)_3(BO_3)_4$ phase (see Fig. 2). Several other compositions in Bi–Cd–B–O and Bi–Al–B–O systems have also been tried, but their powder XRD patterns do not match with that calculated from single-crystal data of $BiCd_3(AlO)_3(BO_3)_4$. Furthermore, several borates including $YCa_3(MO)_3(BO_3)_4$ (M=Mn, Al, and Ga) with Y^{3+}/Ca^{2+} disorder and similar crystal structures have been previously reported (which will be discussed by us later). These support the Bi^{3+}/Cd^{2+} disorder in $BiCd_3(AlO)_3(BO_3)_4$.

2.3. Spectral measurements

Powder XRD data were collected by using the monochromatized Cu$K\alpha$ radiation of a Bruker D8 ADVANCE diffractometer. Infrared spectra were recorded from 4000 to 400 cm^{-1} on a Perkin Elmer 1730 FT-IR spectrometer from KBr pellets. Optical diffuse reflectance spectra were measured at room temperature with a Shimadzu UV-3101PC double-beam, double-monochromator spectrophotometer. Data were collected in the wavelength range 200–1000 nm. $BaSO_4$ powder was used as a standard (100% reflectance). A similar procedure as previously described [23,24] was used to collect and convert the data using the Kubelka–Munk function $F(R)=(1-R)^2/2R$, where R is the reflectance. The minima in the second-derivative curves of the Kubelka–Munk function are taken as the position of the absorption bands. The emission spectrum was measured on an F-7000 time-resolved fluorescence spectrometer using a Xe lamp at room temperature.

2.4. Electronic structure calculations

Energy band, density of states (DOS), and optical property calculations were performed using a first principle plane-wave pseudopotential technique based on density functional theory (DFT) with CASTEP code [25] distributed inside a computational commercial pack [26]. The ion–electron interaction was modeled by an ultrasoft nonlocal pseudopotential [27]. The density functional was treated by the generalized gradient approximation (GGA) with the exchange-correlation potential parametrization (PBE) of Perdew–Burke-Ernzerhof type [28]. Pseudoatomic calculations were performed for Bi $6s^2\ 6p^3$, Cd $4d^{10}\ 5s^2$, Al $3s^2\ 3p^1$, B $2s^2\ 2p^1$, and O $2s^2\ 2p^4$. A kinetic energy cut-off of 300 eV was used for plane wave expansions in reciprocal space. The calculating parameters and convergent criterions were set by the default values of CASTEP code [26]. The calculations of linear optical properties described in terms of the complex dielectric function $\varepsilon=\varepsilon_1+i\varepsilon_2$ were also made in this work. The imaginary part of the dielectric function, $\varepsilon_2(\omega)$, can be described as detailing the real transitions between occupied and unoccupied electronic states. The real and imaginary parts are linked by a Kramers–Kronig transform [29].

Note that Bi and Cd atoms are statistically distributed over the two crystallographic sites, *M*1 [$Bi_{0.2105(6)}Cd_{0.7895(6)}$] and *M*2 [$Bi_{0.3685(18)}Cd_{0.6315(18)}$], which makes electronic structure calculations difficult. In order to perform calculations, we make an assumption that Cd atoms fully occupy *M*1 and Bi atoms fully occupy *M*2 sites, which also results in the formula $BiCd_3Al_3B_4O_{15}$. This assumption is close to the fact that *M*1 has more Cd content and *M*2 contains relatively more Bi component than *M*1.

3. Results and discussion

3.1. Description of the structure

The basic structural units in $BiCd_3(AlO)_3(BO_3)_4$ are AlO_6 octahedra and BO_3 triangles. As seen from Fig. 1(a), each AlO_6^{9-} octahedron is connected to two other octahedra through sharing opposite O···O edges to form one-dimensional (1D) $^1_\infty[AlO_4]^{5-}$ chains extending along the [001] direction. These $^1_\infty[AlO_4]^{5-}$ chains are arranged in a hexagonal way and further bridged by B1-centered BO_3 groups through sharing O atoms to form the 3D $^3_\infty[AlBO_4]^{2-}$ framework. The BO_3 groups and aluminum oxide chains are joined in such a way that two O vertices of each BO_3 triangle are located at the same $^1_\infty[AlO_4]^{5-}$ chain and the third O vertex at the neighboring chain. The 3D framework affords two kinds of open channels running along the [001] direction: the smaller one having a six-sided cross section and the bigger one with a 12-sided window (Fig. 1(b)). The former is only occupied by *M*2 [$Bi_{0.3685(18)}Cd_{0.6315(18)}$] atoms, while the latter is filled by *M*1 [$Bi_{0.2105(6)}Cd_{0.7895(6)}$] atoms and B2-centered BO_3 groups simultaneously. The B2-centered BO_3 triangles go through the centers of the channels and are surrounded by *M*1 atoms. This completes the final structure resulting in the formula $BiCd_3\ [BO_3][AlBO_4]_3$.

As mentioned above, in this structure, Bi and Cd atoms are statistically distributed over the two crystallographic sites, *M*1 [$Bi_{0.2105(6)}Cd_{0.7895(6)}$] and *M*2 [$Bi_{0.3685(18)}Cd_{0.6315(18)}$]. Among them, *M*1 has more Cd content and occupies crystallographic general position, while *M*2 contains relatively more Bi component than *M*1 and lies on a crystallographic three-fold axis. Each *M*1 is coordinated to seven O atoms arranged in a distorted pentagonal bipyramidal geometry with *M*–O distances of 2.246(4)–2.708(6) Å (average 2.417 Å, CN=7, Table 3), while each *M*2 is surrounded by nine O atoms forming a tri-capped trigonal prism with average *M*–O distance being slightly larger than that for the *M*1 atom [*M*2–O=2.259(4)–2.660(11) Å, average 2.483 Å, CN=9]. These *M*–O distances are reasonable when compared with those observed in $Bi_{0.78}Cd_{0.22}VO_{3.72}$ [Bi/Cd–O=2.41(1)–2.52(1) Å, average

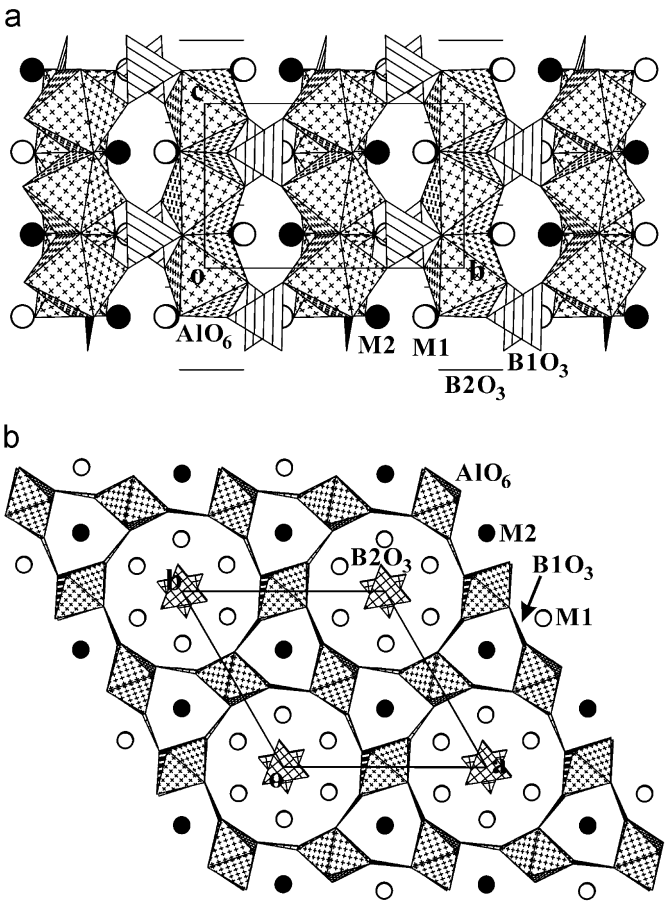

Fig. 1. The crystal structure of $BiCd_3(AlO)_3(BO_3)_4$ projected along the [100] (a) and [001] (b) direction, respectively. *M*1 [$Bi_{0.2105(6)}Cd_{0.7895(6)}$] atoms: open circles; *M*2 [$Bi_{0.3685(18)}Cd_{0.6315(18)}$] atoms: black circles; AlO_6 groups: ctahedral with crosses; $B1O_3$ groups: triangles with parallel lines; $B2O_3$ groups: triangles with grid lines.

Table 3
Selected bond lengths (Å) and angles (deg) for $BiCd_3(AlO)_3(BO_3)_4$.

*M*1–O4	2.246(4)	Al1–O4	1.774(16)
*M*1–O5	2.266(6)	Al1–O4	1.866(16)
*M*1–O3	2.291(10)	Al1–O2	1.922(18)
*M*1–O5	2.336(6)	Al1–O3	1.931(18)
*M*1–O2	2.389(11)	Al1–O1	1.978(15)
*M*1–O1	2.680(4)	Al1–O1	2.033(15)
*M*1–O5	2.708(6)	Mean	1.917
Mean	2.417	B1–O3	1.33(2)
*M*2–O4 × 3	2.259(4)	B1–O1	1.399(7)
*M*2–O2 × 3	2.530(10)	B1–O2	1.42(2)
*M*2–O3 × 3	2.660(11)	Mean	1.383
Mean	2.483	B2–O5 × 3	1.376(6)
O4-Al1-O4	175.3(8)	O4–Al1–O1	79.8(5)
O4–Al1–O2	92.5(5)	O2–Al1–O1	90.3(5)
O4–Al1–O2	88.2(7)	O3–Al1–O1	89.8(6)
O4–Al1–O3	91.5(7)	O1–Al1–O1	179.1(9)
O4–Al1–O3	87.8(5)		
O2–Al1–O3	176.0(8)	O3–B1–O1	121.9(16)
O4–Al1–O1	83.5(6)	O3–B1–O2	120.4(5)
O4–Al1–O1	101.1(6)	O1–B1–O2	117.6(15)
O2-Al1-O1	89.8(7)	Mean	119.97
O3–Al1–O1	90.1(5)	O5–B2–O5 × 3	119.54(13)
O4–Al1–O1	95.6(6)		

2.448−2.460 Å, CN=8] [19] and $Bi_{3.785}Cd_{3.3}Cu_{1.775}(PO_4)_{3.5}O_{5.5}$ [Bi/Cd–O=2.23(4)–2.98(3) Å, average 2.477 Å, CN=9] [22]. Both *M*1–O and *M*2–O ctahedral are only slightly distorted, implying that the lone-pair on Bi^{3+} is inert rather than stereo-active. This may be due to the fact that Bi and Cd atoms are disordered, which limits the stereo-activity of Bi^{3+} $6s^2$ electron lone pairs. There is one crystallographically unique Al atom, which has six O nearest-neighbors arranged into a slightly distorted octahedron, with the 180° octahedral angles being 175.3(8)–179.1(9)°, and the 90° octahedral angles in the range 79.8(5)–95.6(6)°. Al–O bond lengths are normal, lying in the range 1.774(16)–2.033(15) (average 1.917 Å). Similar Al(III) coordination geometries have been encountered in the structures of $AlBO_3$ (average Al–O= 1.923 Å, CN=6) [30] and $TmAl_3(BO_3)_4$ (average Al–O=1.901 Å, CN=6) [31]. A bond valence sum [32] of 2.96 can be computed for the Al atom, supporting the choice of six-fold coordination to describe the Al environment. Of the two independent B atoms, B1 occupies crystallographic general position and B2 is located on a crystallographic three-fold axis. The B1- and B2-centered BO_3 groups are oriented with their triangular faces parallel and perpendicular to the [001] direction, respectively. The O–B–O bond angles are 117.6(15)–121.9(16)° for B1 and $3\times119.54(13)$° for B2, indicating that the triangular coordination around the B atom is approximately planar. The B–O bond lengths range from 1.33(2) to 1.42(2) Å with average values of 1.376–1.383 Å, which are comparable to those reported in other orthoborates, e.g., $AlBO_3$ [1.380(1) Å] [30], $FeBO_3$ [1.379(2) Å] [33], $InBO_3$ [1.380(1) Å] [34], $LuBO_3$ [1.370(1) Å] [35], and $ScBO_3$ [1.375(1) Å] [36]. Bond valence analyses gave values of 2.92–2.96 for the B atoms, in good agreement with their expected formal valences.

$BiCd_3(AlO)_3(BO_3)_4$ is isostructural with Gaudefroyite, $Ca_4(MnO)_3(BO_3)_3CO_3$. That mineral was first reported by Jouravsky and Permingeat [37]. Its crystal structure was subsequently determined by Yakubovich et al. in a non-centrosymmetric group $P6_3$ and by Hoffmann et al. and Antao et al. in a centrosymmetric group $P6_3/m$, respectively [38–40]. The crystal structure contains MnO_6 octahedral chains that are interlinked by BO_3 groups to form a Kagomé network, with the trigonal and apatitelike channels in the network hosting Ca^{2+} ions only and hosting Ca^{2+} ions together with CO_3^{2-} groups, respectively. When the CO_3^{2-} group in gaudefroyite, $Ca_4(MnO)_3(BO_3)_3CO_3$, is replaced by another BO_3^{3-} group and one Ca^{2+} ion simultaneously substituted by a Y^{3+} ion to provide charge balance, $Yca_3(MnO)_3(BO_3)_4$ is obtained [41]. Further replacing Mn^{3+} in $Yca_3(MnO)_3(BO_3)_4$ with Al^{3+} and Ga^{3+} ions results in the formation of $Yca_3(AlO)_3(BO_3)_4$ and $Yca_3(GaO)_3(BO_3)_4$, respectively [42]. These three borates are all isostructural with Gaudefroyite and their crystal structures have been refined in the $P6_3/m$ group from powder diffraction data using the Rietveld method, where the Y^{3+}/Ca^{2+} disorder and B and O disorder were reported. Our attempts to refine the present single-crystal data in the $P6_3/m$ group led to the residuals close to those for the $P6_3$ group. However, like the situation in $Yca_3(MO)_3(BO_3)_4$ (*M*=Mn, Al, and Ga), one B and one O atoms in the asymmetric unit were found to be disordered with occupation factors of 1/2 accompanied by very close B–B and O–O bond distances [B2–B2=0.79 (4) Å and O4–O4=1.65 (1) Å, respectively]. In contrast, the refinements in the $P6_3$ group produced more reasonable results, which gave an ordered distribution of B and O atoms and no unusual short B–B and O–O bonds were found. Positional parameters of the title compound (Table 2) have also been checked using the program MISSYM [43], no potential additional symmetry was found, confirming the $P6_3$ model.

The title compound crystallizes in the polar space group $P6_3$, which is in the crystal class 6 and should display NLO effect. To confirm this, SHG measurements were performed using a Kurtz-NLO system [44] on the powder sample. Fundamental 1064 nm light was generated with a Q-switched Nd:YAG laser. Microcrystalline KDP (KH_2PO_4) served as the standard. Both the sample and KDP reference were ground and sieved and powders with particle sizes of 76–100 μm were used for comparing SHG intensities. Green light of 532 nm was clearly observed and its intensity was about 0.5 times of that of KDP (KH_2PO_4), further supporting the assignment of this structure in a non-centrosymmetric setting.

3.2. Spectrum properties

Fig. 2 shows the XRD pattern of $BiCd_3(AlO)_3(BO_3)_4$ obtained from powder diffractometer data, together with that calculated from the single crystal data for comparison. It is clear that the observed diffraction peak positions match with the calculated ones, confirming the phase purity. Note that the observed XRD pattern contains weak additional peaks in comparison to the calculated one. These additional peaks match those of AlO(OH) (JCPDS card 72-1268) and CdB_4O_7 (JCPDS card 71-2169). Because it takes a long time for a solid state reaction to be finished, the formation of intermediate compounds or other thermodynamically stable phases are understandable.

Concerning IR spectra of borates it is reported [5] that the frequencies of normal vibrations of BO_3 groups lie in the ranges $\nu_s\sim$850–960 cm^{-1}, $\gamma\sim$650–800 cm^{-1}, $\nu_{as}\sim$1100–1450 cm^{-1}, and $\delta\sim$500–600 cm^{-1}. Infrared spectrum of the titled compound was shown in Fig. 3, where the bands at around 1277.6 cm^{-1} may be assigned as the BO_3 antisymmetric stretching vibrations (ν_{as}); the bands in the frequency range 664.2–738.4 cm^{-1} caused by the out-of-plane bending vibrations (γ); bands at about 549.0 cm^{-1} due to the in-plane bending modes (δ), and those below 500 cm^{-1} attributed to lattice vibrations. The IR spectrum confirms the existence of only trigonally coordinated boron atoms, consistent with the results obtained from the crystallographic study.

The optical diffuse reflectance spectrum is shown in Fig. 4. It is observed that $BiCd_3(AlO)_3(BO_3)_4$ has no absorption above 400 nm, implying that the material is transparent under the visible light, while at around 288 nm this compound has strong absorption. From the absorption edge of UV–vis diffuse reflectance spectrum (389.2 nm), the optical band gap is estimated to be roughly 3.19 eV. In addition, the emission spectrum of $BiCd_3(AlO)_3(BO_3)_4$ was recorded when an ultraviolet light of 300 nm is used to excite

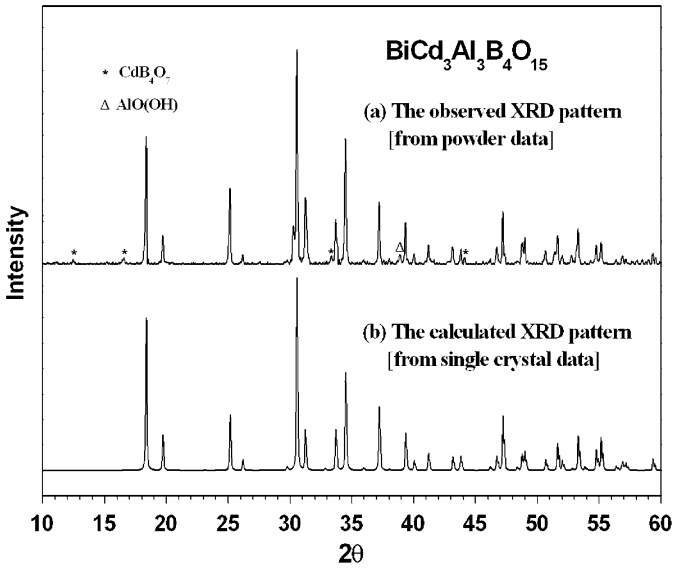

Fig. 2. XRD patterns of $BiCd_3(AlO)_3(BO_3)_4$ observed from powder polycrystalline sample (a) and calculated from the single-crystal data (b).

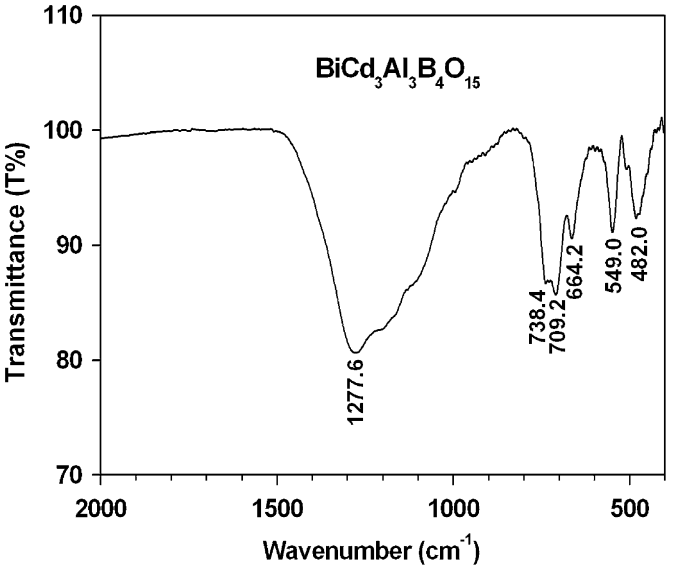

Fig. 3. Infrared spectrum of $BiCd_3(AlO)_3(BO_3)_4$.

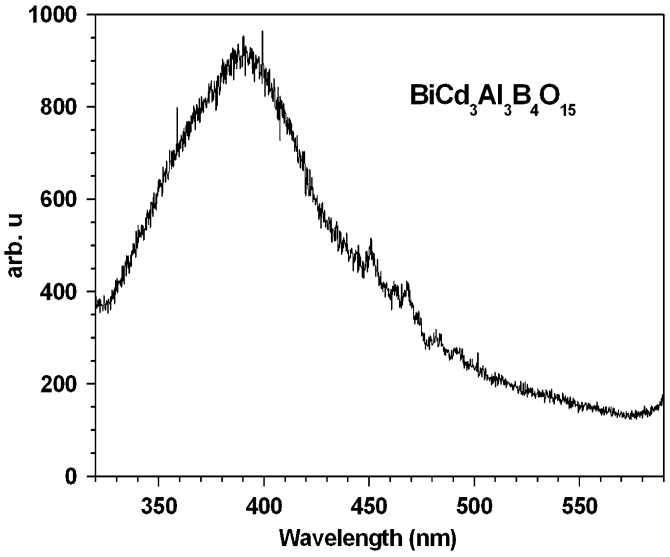

Fig. 5. Emission spectrum of $BiCd_3(AlO)_3(BO_3)_4$.

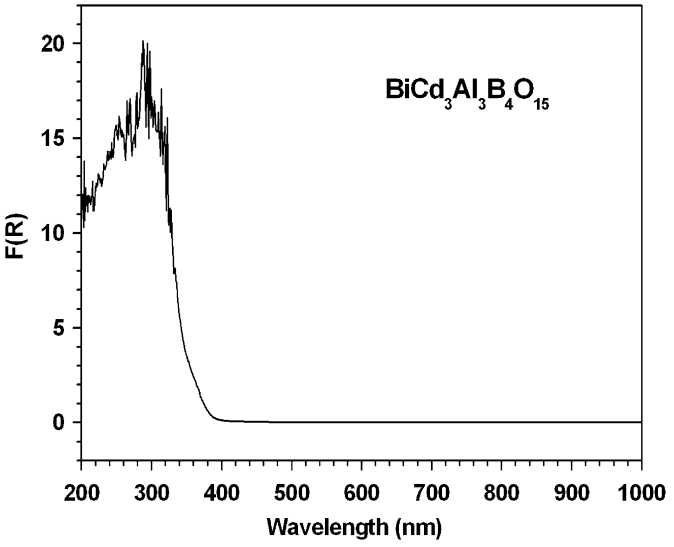

Fig. 4. Optical absorption spectrum of $BiCd_3(AlO)_3(BO_3)_4$.

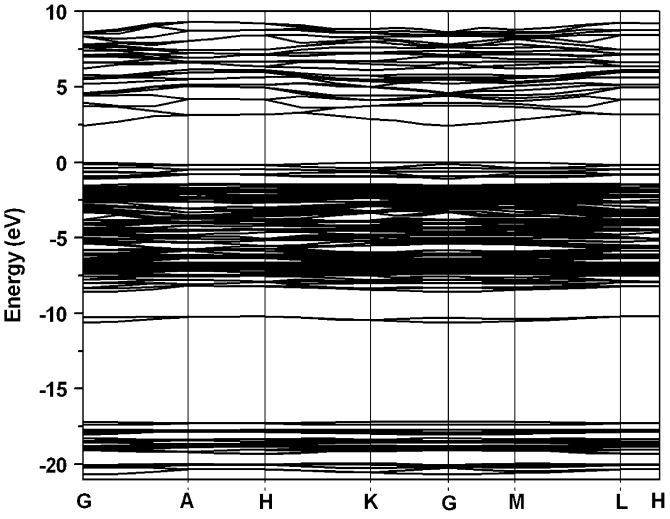

Fig. 6. The calculated band structure of $BiCd_3(AlO)_3(BO_3)_4$, where the Fermi level (E_F) is set at 0 eV and the labeled k-points are present as G (0, 0, 0), A (0, 0, 1/2), H (−1/3, 2/3, 1/2), K (−1/3, 2/3, 0), M (0, 1/2, 0), and L (0, 1/2, 1/2).

it. A broad emission band at around 390.6 nm (3.17 eV) is observed, as shown in Fig. 5. Since the emission energy of 3.17 eV is slightly less than the optical absorption edge of 3.19 eV, we can deduce that the emitted fluorescence probably originates from the defects or excitons.

3.3. Band structures, densities of states, and optical properties

The calculated band structure of $BiCd_3(AlO)_3(BO_3)_4$ along high-symmetry points of the first Brillouin zone is shown in Fig. 6. It is observed that the valence band maximum (VBM) is located at halfway between K and the G point, and the conduction band minimum (CBM) is located at the G point, resulting in an indirect energy gap of 2.44 eV. The calculated energy gap is smaller than the corresponding experimental value of 3.19 eV as the generalized gradient approximation (GGA) generally underestimates the size of the band gap.

The bands can be assigned according to the total and partial densities of states (TDOS, PDOS) as plotted in Fig. 7. For $BiCd_3(AlO)_3(BO_3)_4$, the band structure can be divided into four principal groups separated by gaps. The lowest group is located at the energy range from −21.2 to −16.5 eV, which mainly originates from O 2*s* states, with small admixtures of B 2*s*/2*p* and Al 3*s*/3*p* states. The second group lying around −10.3 eV is derived from Bi 6*s* orbitals, with small contributions of O 2*p* component. The group from −9.1 eV up to Fermi energy (E_F) is mainly of Cd 4*d* and O 2*p* character, with small admixtures of B 2*s*/2*p*, Al 3*s*/3*p*, and Bi 6*s*/6*p* states. The group from the CBM up to 8.0 eV is dominated by the Bi 6*s*/6*p*, B 2*p*, and Cd 5*s*/5*p* states, mixing with small amounts of O 2*p* states. The electronic structure of the upper valence band is dominated by the O 2p and Bi 6*s* states. We note that most of the O 2*p* character is concentrated in the upper valence band, with only negligible amounts in the conduction band. The CBM is controlled by Bi 6*p* states.

From the PDOS, we note a strong hybridization between B 2*s*/2*p* and O 2*p* and between Al 3*s*/3*p* and O 2*p* states in the energy region from −9.0 eV to E_F, implying that the substantial covalence interactions exist between B and O and between Al and O atoms.

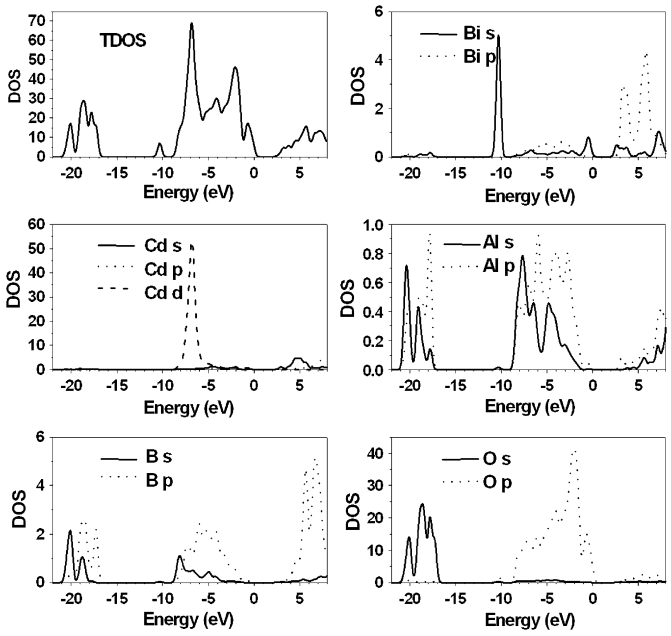

Fig. 7. Total and partial densities of states of $BiCd_3(AlO)_3(BO_3)_4$.

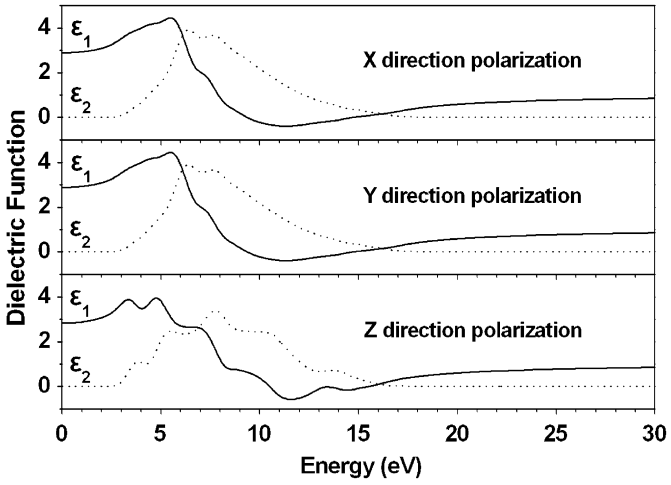

Fig. 8. Calculated real and imaginary parts of dielectric functions in different polarization directions for $BiCd_3(AlO)_3(BO_3)_4$.

This is also reflected by population analyses. The calculated bond orders of B–O, Al–O, and Bi/Cd–O bonds in a unit cell are 0.83–0.91e, 0.29–0.44e, and −0.02–0.19e, respectively. Accordingly, we can say that the covalent strength of B–O bonds is stronger than that of Al–O bonds, and the ionic character of Bi/Cd–O bonds is larger than that of the Al–O bonds.

Fig. 8 displays calculated real (ε_1) and imaginary (ε_2) parts of dielectric functions of $BiCd_3(AlO)_3(BO_3)_4$ in different polarization directions without the DFT scissor operator approximation. The spectral broadening is taken to be 0.4 eV. It can be seen from the $\varepsilon_2(\omega)$ curves that there are three absorption peaks at the lower energy region: the weak one at about 3.85 eV and two strong ones at about 5.49 and 7.74 eV in the *z* polarization direction (which correspond to those at about 6.38 and 7.60 eV in the *x* polarization direction). The peak in $\varepsilon_2(\omega)$ can correspond to electronic transitions with the same energy between the occupied and unoccupied bands. Therefore, two strong absorption peaks in the $\varepsilon_2(\omega)$ curves are assigned as the electronic transitions from the occupied O 2*p* states to the mixed states of unoccupied B 2*p*, Bi 6*p*, and Cd 5*s* orbitals and to the mixed states of unoccupied B 2*p*, Bi 6*s*/6*p*, and Cd 5*p* orbitals, respectively, in terms of total and partial DOS analyses. The weak peak at about 3.85 eV corresponds to that at around 4.30 eV (288 nm) of the experimental spectrum (Fig. 4), which is assigned as the electronic transitions from the O 2*p* to Bi 6*p* states.

From the spectral dependences of imaginary parts of the dielectric function $\varepsilon_2(\omega)$ the real parts $\varepsilon_1(\omega)$ can be calculated using Kramers–Kronig relations [29]. The static dielectric constant $\varepsilon(0)$ is given by the low energy limit of $\varepsilon_1(\omega)$ [$\varepsilon(0) \approx \varepsilon_1(0)$ at low frequency]. The calculated value of $\varepsilon(0)$ is about 2.880, 2.880 and 2.829 along the *x*, *y* and *z* directions, indicating a strong anisotropy of the dielectric function. The refractive index is an important optical parameter in optical transmitted materials. It is a measure of how faster light travels in a medium and the lower the refractive index, the faster the speed of light. The knowledge of both real and imaginary parts of the frequency dependent dielectric function allows the calculations of the dispersion curves of refractive index by the relation of $n^2(\omega)=\varepsilon(\omega)=\varepsilon_1(\omega)+i\varepsilon_2(\omega)$. Based on the $n(\omega)$ curves, the refractive indexes of n_x, n_y and n_z were found to be 1.715, 1.715 and 1.703 at the wavelength of 1064 nm, respectively. Although the refractive indices of $BiCd_3(AlO)_3(BO_3)_4$ have not been measured, our calculated results are reasonable when compared with the observed values of other borates which are generally in the range 1.43–1.75 [45–48].

4. Conclusions

A novel quaternary borate, $BiCd_3(AlO)_3(BO_3)_4$, has been synthesized and characterized. It crystallizes in the hexagonal space group $P6_3$ and has a 3D network formed by stitching 1D chains of edge-sharing AlO_6 octahedra *via* the bridging BO_3 groups. There are two types of channels in the network that are filled by Bi^{3+}/Cd^{2+} atoms only or by Bi^{3+}/Cd^{2+} atoms together with BO_3 groups. The optical properties have been investigated in terms of diffuse reflectance and fluorescent spectra, which reveal the presence of an optical gap of 3.19 eV and a broad emission band in the solid-state at around 390.6 nm upon photoexcitation at 300 nm. Band structure calculations with CASTEP code show that this compound has an indirect energy gap of 2.44 eV, which is smaller than our measured value as expected from GGA calculations. The top of the valence band mainly originates from the O 2*p* states and the bottom of the conduction band primarily from Bi 6*p* states. The electronic transitions from the O 2*p* to Bi 6*p* states make the main contribution to the optical absorption edge of $BiCd_3(AlO)_3(BO_3)_4$. In addition, dielectric constants and refractive indexes have also been calculated and the refractive indexes derived from dielectric constant are close to the observed values of other borates.

Acknowledgment

This work was supported by the National Natural Science Foundation of China (Grant no. 20871012).

Appendix A. Supporting information

Supplementary data associated with this article can be found in the online version at doi:10.1016/j.jssc.2010.09.030.

References

[1] P. Becker, Adv. Mater. 10 (1998) 979.
[2] E.M. Levin, C.L. McDaniel, J. Am. Ceram. Soc. 45 (1962) 355.

[3] Y.F. Kargin, A.V. Egorysheva, Inorg. Mater. 34 (1998) 714.
[4] A. Hyman, A. Perloff, Acta Crystallogr. B 28 (1972) 2007.
[5] S. Filatov, Y. Shepelev, R. Bubnova, N. Sennova, A.V. Egorysheva, Y.F. Kargin, J. Solid State Chem. 177 (2004) 515.
[6] R. Frohlich, L. Bohaty, J. Liebertz, Acta Crystallogr. C 40 (1984) 343.
[7] B. Teng, W.T. Yu, J.Y. Wang, X.F. Cheng, S.M. Dong, Y.G. Liu, Acta Crystallogr. C 58 (2002) i25.
[8] R.S. Bubnova, J.V. Alexandrova, S.V. Krivovichev, S.K. Filatov, A.V. Egorysheva, J. Solid State Chem. 183 (2010) 458.
[9] M. Muehlberg, M. Burianek, H. Edongue, C. Poetsch, J. Cryst. Growth 237–239 (2002) 740.
[10] A.V. Egorysheva, V.I. Burkov, V.S. Gorelick, Yu.F. Kargin, V.V. Koltashev, B.G. Plotnichenko, Fiz. Tverd. Tela 43 (9) (2001) 1590 (Phys. Solid State 43 (2001) 1655, English translation).
[11] G. Blasse, E.W.J.L. Oomen, J. Liebertz, Phys. Stat. Sol. (b) 137 (1986) K77.
[12] S. Haussühl, L. Bohatý, P. Becker, Appl. Phys. A 82 (2006) 495.
[13] D. Xue, K. Betzler, H. Hesse, D. Lammers, Phys. Stat. Sol. (A) 176 (1999) R1.
[14] J. Barbier, N. Penin, A. Denoyer, L.M.D. Cranswick, Solid State Sci. 7 (2005) 1055.
[15] J. Barbier, N. Penin, L.M. Cranswick, Chem. Mater. 17 (2005) 3130.
[16] J. Barbier, L.M.D. Cranswick, J. Solid State Chem. 179 (2006) 3958.
[17] G.M. Sheldrick, SHELX-97: program for structure refinement, University of Goettingen, Germany, 1997.
[18] S.D. Kirik, L.S. Tsurgan, G.G. Pervyshina, T.I. Koryagina, V.A. Kutvitskii, Sov. Phys. Crystallogr. 37 (1992) 761.
[19] S. Uma, R. Bliesner, A.W. Sleight, Solid State Sci. 4 (2002) 329.
[20] O. Labidi, M. Drache, P. Roussel, J.-P. Wignacourt, Solid State Sci. 9 (2007) 964.
[21] O. Labidi, M. Drache, P. Roussel, J.-P. Wignacourt, Solid State Sci. 10 (2008) 1074.
[22] M. Colmont, M. Huve, F. Abraham, O. Mentre, J. Solid State Chem. 177 (2004) 4149.
[23] J. Li, Z. Chen, X.-X. Wang, D.M. Proserpio, J. Alloys Compd. 262–263 (1997) 28.
[24] W.W.M. Wendlandt, H.G. Hecht, Reflectance Spectroscopy, Interscience: A Division of John Wiley & Sons, New York, 1966.
[25] M.C. Payne, M.P. Teter, D.C. Allan, T.A. Arias, J.D. Joannopoulos, Rev. Mod. Phys. 64 (1992) 1045.
[26] Materials Studio, Version 4.1, Accelrys Inc., San Diego, 2006.
[27] D. Vanderbilt, Phys. Rev. B 41 (1990) 7892.
[28] J.P. Perdew, K. Burke, W. Ernzerhof, Phys. Rev. Lett. 77 (1996) 3865.
[29] J.R. Macdonald, M.K. Brachman, Rev. Mod. Phys. 28 (1956) 383.
[30] A. Vegas, Acta Crystallogr. B33 (1977) 3607.
[31] G. Jia, C. Tu, J. Li, Z. You, Z. Zhu, B. Wu, Inorg. Chem. 45 (2006) 9326.
[32] I.D. Brown, D. Altermatt, Acta Crystallogr. B 41 (1985) 244.
[33] J.R. Cox, D.A. Keszler, Acta Crystallogr. C 50 (1994) 1857.
[34] R. Diehl, Solid State Commun. 17 (1975) 743.
[35] D.A. Keszler, H. Sun, Acta Crystallogr. C44 (1988) 1505.
[36] S.C. Abrahams, J.L. Bernstein, E.T. Keve, J. Appl. Crystallogr. 4 (1971) 284.
[37] G. Jouravsky, F. Permingeat, Bull. Soc. Fr. Mineral. Cristallogr. 87 (1964) 216.
[38] O.V. Yakubovich, M.A. Simonov, N.V. Belov, Sov. Phys. Crystallogr. 20 (1975) 87.
[39] C. Hoffmann, T. Armbruster, M. Kunz, Eur. J. Mineral. 9 (1997) 7.
[40] S.M. Antao, I. Hassan, Can. Mineral. 46 (2008) 183.
[41] R.K. Li, C. Greaves, Phys. Rev. B 68 (2003) 172403.
[42] Yi Yu, Q.S. Wu, R.K. Li, J. Solid State Chem. 179 (2006) 429.
[43] Y. Le Page, J. Appl. Crystallogr. 20 (1987) 264.
[44] S.K. Kurtz, T.T. Perry, J. Appl. Phys. 39 (1968) 3798.
[45] S.Y. Zhang, X. Wu, Y.T. Song, D.Q. Ni, B.Q. Hu, T. Zhou, J. Cryst. Growth 252 (2003) 246.
[46] T. Sasaki, Y. Mori, M. Yoshimura, Opt. Mater. 23 (2003) 343.
[47] G. Ryu, C.S. Yoon, T.P.J. Han, H.G. Gallagher, J. Cryst. Growth 191 (1998) 492.
[48] S.F. Wu, G.F. Wang, J.L. Xie, X.Q. Wu, Y.F. Zhang, X. Lin, J. Cryst. Growth 245 (2002) 84.